Supplementary Information

Dynamically Stable and Amplified Circularly Polarized Excimer Emission (CPEE) of Achiral Pyrene-Based Dye Regulated by Solvation of Chiral Co-assembly Process

*Yuxia Zhang,[a] Hang Li,[a] Zhongxing Geng,[b] Wen-hua Zheng, *[a] Yiwu Quan*[b] and Yixiang Cheng*[a]*

a. Jiangsu Key Laboratory of Advanced Organic Materials, School of Chemistry and Chemical Engineering, Nanjing University, Nanjing 210023, China. E-mail: yxcheng@nju.edu.cn. E-mail: wzheng@nju.edu.cn.

b. Key Laboratory of High Performance Polymer Material and Technology of Ministry of Education, Department of Polymer Science and Engineering, School of Chemistry and Chemical Engineering, Nanjing University, Nanjing 210023, China. E-mail: quanyiwu@nju.edu.cn

Table of Contents

1. Measurements and materials.

All NMR spectra were obtained by using a Bruker (400 MHz) spectrometer. Chemical shifts were recorded as parts per million (ppm, δ) relative to tetramethylsilane (δ 0.00) or chloroform (δ = 7.26, singlet). ^{1}H NMR splitting patterns are designated as singlet (s), doublet (d), triplet (t), multiplets (m) and etc. Ultraviolet-visible (UV-*vis*) spectra were measured by using a Shimadzu UV-3600 spectrophotometer. Fluorescence spectra were tested from a HORIBA Scientific FluoroMax-4 Spectrofluorometer. X-ray diffraction (XRD) was measured by using Rigaku D/Max-2500 X-ray diffractometer (Japan) with Cu/Kα radiation (λ = 1.5406 Å), which was operated at a voltage of 40 kV and a current of 200 mA. The absolute PL quantum yield were measured by a HORIBA Fluorolog-3 3D-Spectrofluorometer. Circular dichroism (CD) spectra were performed on a JASCO J-810 spectropolarimeter. CPL spectra were collected on a JASCO CPL-300 spectrofluoropolarimeter. In the CPL measurements, scan speed was 200 nm/min, number of scans was 1, and slit width was 3000 μm. Scanning electron microscope (SEM) images were taken in Hitachi S-4800 field emission scanning electron microscopy. The liquid crystalline textures were investigated and photographed using liquid crystal cells with a polarized optical microscope (POM) equipped with a Leitz-350 heating stage and an associated Nikon (D3100) digital camera. All solvents and reagents were commercially available A.R. grade.

2. Synthesis and characterizations

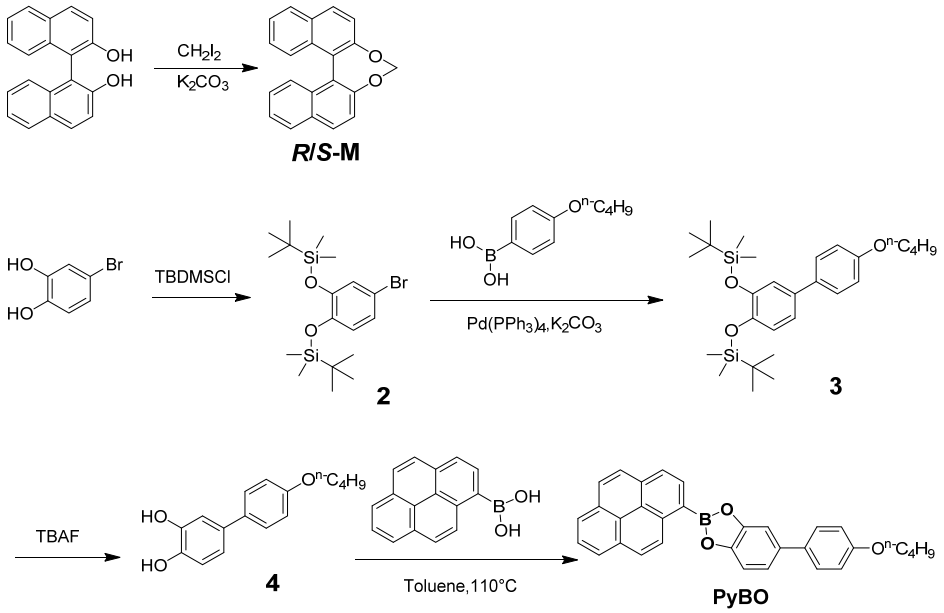

a) Synthesis and characterizations of *R*-/*S*-M.

***R*/*S*-M** were synthesized according to the literature. [1,2]

b) Synthesis and characterizations of 2. [3]

To a solution of the 4-bromocatechol (1.0 equiv) in CH_2Cl_2 was slowly added imidazole (2.4 equiv) at 0℃. After stirring for 20 min, to the mixture was slowly added tert-Butyldimethylsilyl chloride (3.0 equiv) at the same temperature. After being stirred for 4h at room temperature (detected by TLC), the reaction mixture was poured into water to quench the reaction and extracted with CH_2Cl_2. The combined organic layer was washed with brine, dried over Na_2SO_4 and the solvent removed under reduced pressure. The crude product was purified by flash column chromatography (silica gel) to afford the compound **2** as colorless oil (91% yield). ^{1}H NMR ($CDCl_3$, 400 MHz) δ (ppm): 6.95 (d, J = 2.4 Hz, 1H), 6.93-6.90 (m, 1H), 6.69 (d, J = 8.4 Hz, 1H), 0.98 (d, J = 3.6 Hz, 18H), 0.19 (d, J = 7.6 Hz, 12H).

c) Synthesis and characterizations of 3 and 4.

Under Ar atmosphere, to a solution of the compound **2** (1.0 equiv), corresponding boronic acid/esters (1.5 equiv) and $Pd(PPh_3)_4$ (4 mol%) were added toluene (7 mL/mmol), aqueous Na_2CO_3 solution (2.0 M, 3.2 mL/mmol) and ethanolic (3.2 mL/mmol), and the resulting suspension was refluxed until the reaction was completed (detected by TLC). After cooling to room temperature, EA and H_2O were added. The organic phase was separated, washed with brine, dried over Na_2SO_4 and the solvent removed under reduced pressure. The crude product was purified by flash column chromatography (silica gel) to afford the compound **3** (85% yield). The compound **3** was directly diluted in anhydrous THF. TBAF was added (1.0 M in THF, 3.0 equiv) the mixture at ice-water and the reaction mixture was stirred for 4 h at room temperature (detected by TLC). The reaction was quenched by addition of MeOH, and the solvent was removed under reduced pressure. The crude product was recrystallized by using DCM/PE afford the compound **4** (>90% yield). ^{1}H NMR ($CDCl_3$, 400 MHz) δ (ppm): 7.42 (d, J = 8.8 Hz, 2H), 7.07 (d, J = 2.4 Hz, 1H), 7.00 (dd, J = 8.0, 2.0 Hz, 1H), 6.94-6.89 (m, 3H), 5.17 (s, 1H), 5.09 (s, 1H), 3.99 (t, J = 6.4 Hz, 2H), 1.82-1.75 (m, 2H), 1.55-1.46 (m, 2H), 0.99 (t, J = 7.2 Hz, 3H); ^{13}C{^{1}H} NMR ($CDCl_3$, 100 MHz) δ (ppm): 158.4, 143.7, 142.6, 134.5, 133.1, 127.7, 119.4, 115.7, 115.6, 114.8, 113.9, 67.9, 31.4, 19.3, 13.9.

d) Synthesis and characterizations of PyBO.

1-Pyrenylboronic acid (1.0 equiv, 100 mg) and compound **4** were dissolved in dry toluene (5 mL) and the mixture was refluxed at 110 ℃ in dark conditions for 48 h (the fluorescence of the reaction mixture became green-yellow color from blue-purple color). The toluene was removed under reduced pressure and the crude product was washed by

using n-hexane to afford **PyBO** as solid. ^{1}H NMR ($CDCl_3$, 400 MHz) δ (ppm): 9.24 (d, J = 9.2 Hz, 1H), 8.84 (d, J = 7.6 Hz, 1H), 8.29-8.23 (m, 4H), 8.15 (dd, J = 26.8, 8.8 Hz, 2H), 8.06 (t, J = 7.6 Hz, 1H), 7.62 (d, J = 1.6 Hz, 1H), 7.57-7.54 (m, 2H), 7.46 (d, J = 8.4 Hz, 1H), 7.37 (dd, J = 8.4, 2.0 Hz, 1H), 7.02-6.99 (m, 2H), 4.03 (t, J = 6.8 Hz, 2H), 1.85-1.78 (m, 2H), 1.58-1.49 (m, 2H), 1.01 (t, J = 7.2 Hz, 3H); ^{13}C{^{1}H} NMR ($CDCl_3$, 100 MHz) δ (ppm): 158.7, 149.0, 147.6, 136.7, 136.6, 134.4, 134.3, 133.3, 131.1, 130.7, 129.3, 128.7, 128.2, 127.4, 127.3, 126.0, 125.9, 125.8, 124.5, 124.4, 124.3, 121.5, 114.9, 112.5, 111.1, 67.8, 31.4, 19.3, 13.9.

3. UV-*vis* and FL spectra of *R*-M, PyBO and *R*-M-PyBO.

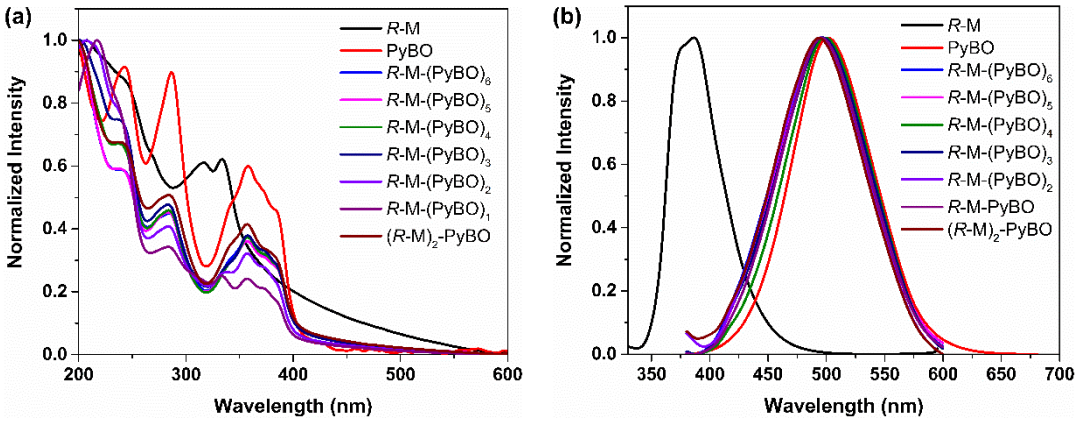

Figure S1. (a) UV-*vis* spectra and (b) FL spectra of ***R*-M, PyBO** and ***R*-M-PyBO** in the spin-coated film.

4. CD and CPL spectra of *R/S*-M-PyBO.

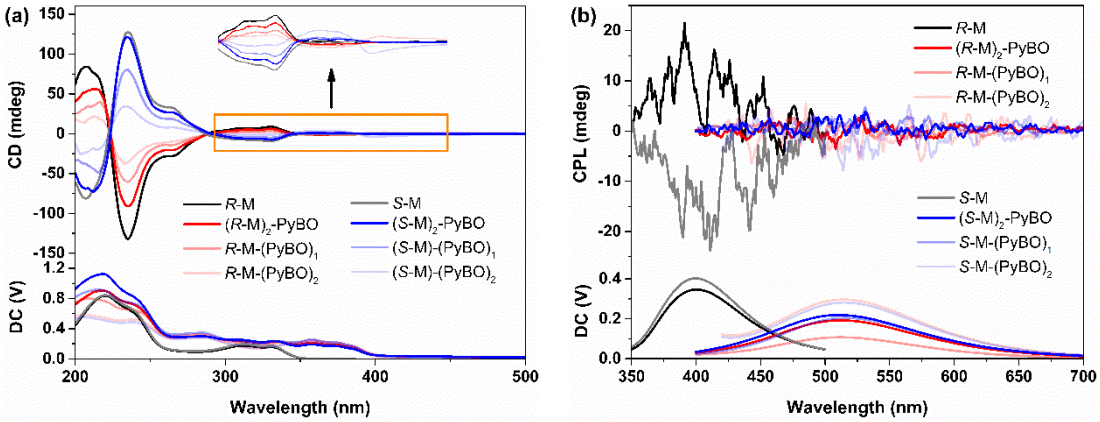

Figure S2. (a) CD spectra and (b) CPL spectra of ***R/S*-M-PyBO** with different molar ratios in the spin-coated film.

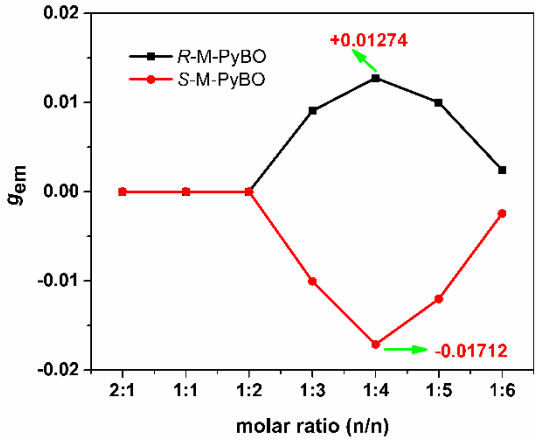

Figure S3. Plot of blend g_{em} values vs the doped concentration molar ratio of ***R/S*-M-PyBO** in the spin-coated film.

5. The g_{em} values of different film thickness of *R/S*-M-(PyBO)$_4$.

Table S1 the g_{em} values of different film thickness of ***R/S*-M-(PyBO)$_4$**.

Concentration (mg/mL)[a]	Film Thickness (nm)	g_{em}
10 (*R*)	35	+ 0.015
20 (*R*)	60	+ 0.110
30 (*R*)	95	+ 0.092
40 (*R*)	130	+ 0.446
50 (*R*)	160	+ 0.210
40 (*S*)	130	- 0.475

[a] The concentration of the toluene solution of ***R/S*-M-(PyBO)$_4$**

6. CPL spectra of *R/S*-M-(PyBO)$_4$.

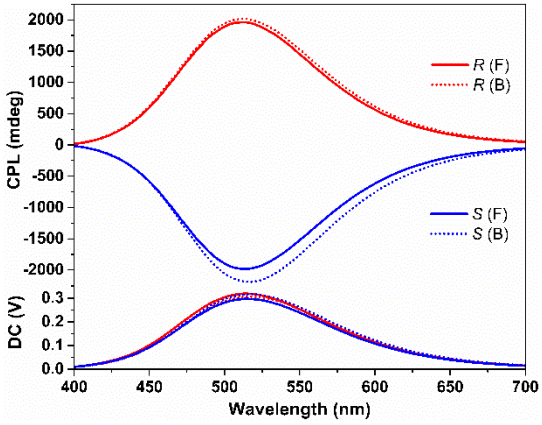

Figure S4. CPL spectra of ***R/S*-M-(PyBO)$_4$** fresh film at 130 nm thickness (the films facing toward the detector: "Frontward", F; away from the detector: "Backward", B).

7. The pictures under UV light and plot of maximum emission wavelength of *R/S*-M-(PyBO)$_4$ versus time.

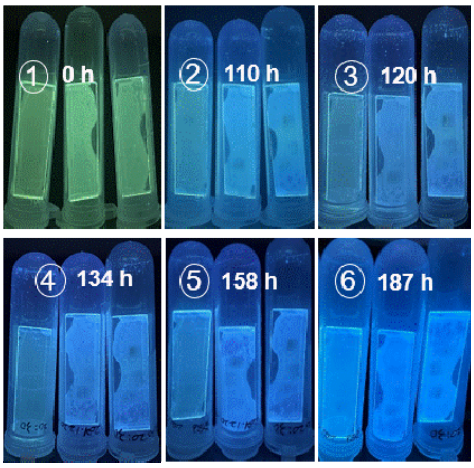

Figure S5. The pictures of **PyBO** (left), ***R*-M-(PyBO)$_4$** (middle) and ***S*-M-(PyBO)$_4$** (right) under UV light in air for different times.

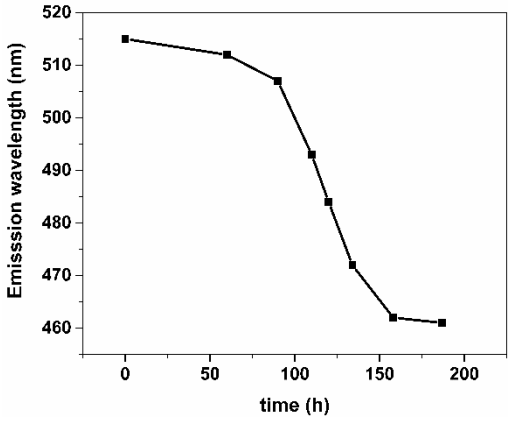

Figure S6. The plot of maximum emission wavelength of ***R*-M-(PyBO)$_4$** versus time.

8. POM and Optical microscope images of *R/S*-M and PyBO films spin-coated from toluene solution.

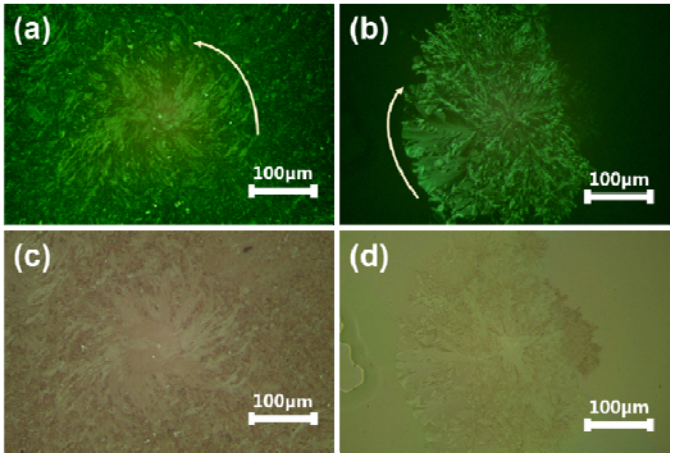

Figure S7. (a) POM images and (c) Optical microscope images of ***R*-M**; (b) POM images and (d) Optical microscope images of ***S*-M**. (spin-coated films after 20 min).

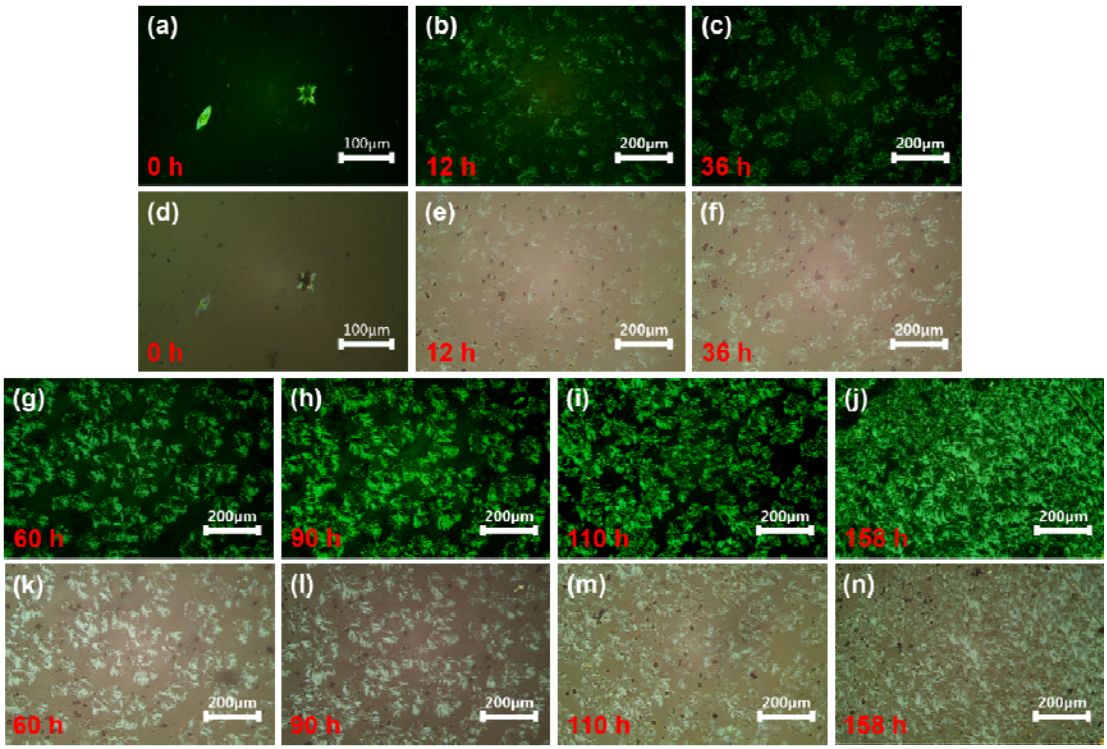

Figure S8. (a-c, g-j) POM images and (d-f, k-n) Optical microscope images of **PyBO**. All films were spin-coated from toluene solutions (40 mg/mL) on quartz plates (1 cm × 3 cm) (1000 N/s, 30 s).

9. The plot of maximum emission wavelength of *R*-M-(PyBO)$_4$ versus spherulite diameters.

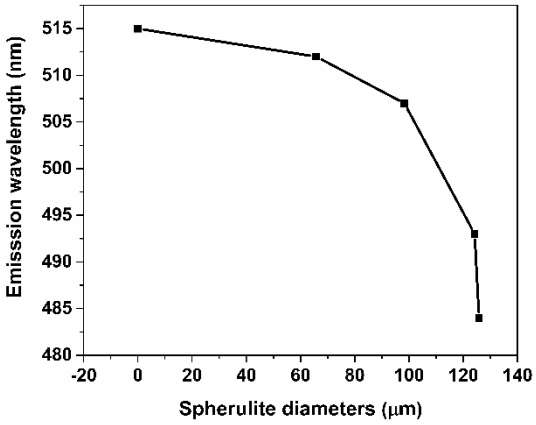

Figure S9. The plot of maximum emission wavelength of ***R*-M-(PyBO)$_4$** versus spherulite diameters.

10. CPL spectra of *R*-M-(PyBO)$_4$-D/T.

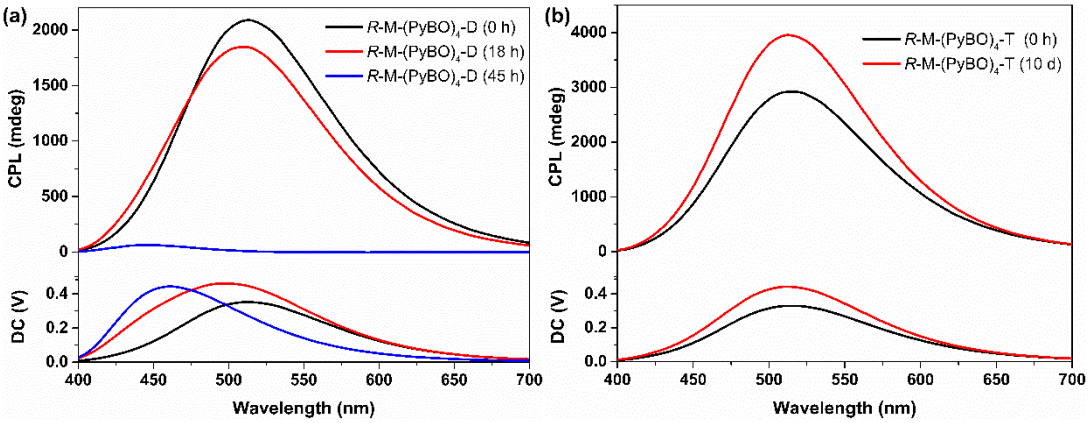

Figure S10. CPL spectra of (a) ***R*-M-(PyBO)$_4$-D** and (b) ***R*-M-(PyBO)$_4$-T** at different time. All spin-coated films from 40 mg/mL solutions on quartz plates (1 cm × 3 cm) (1000 N/s, 30 s).

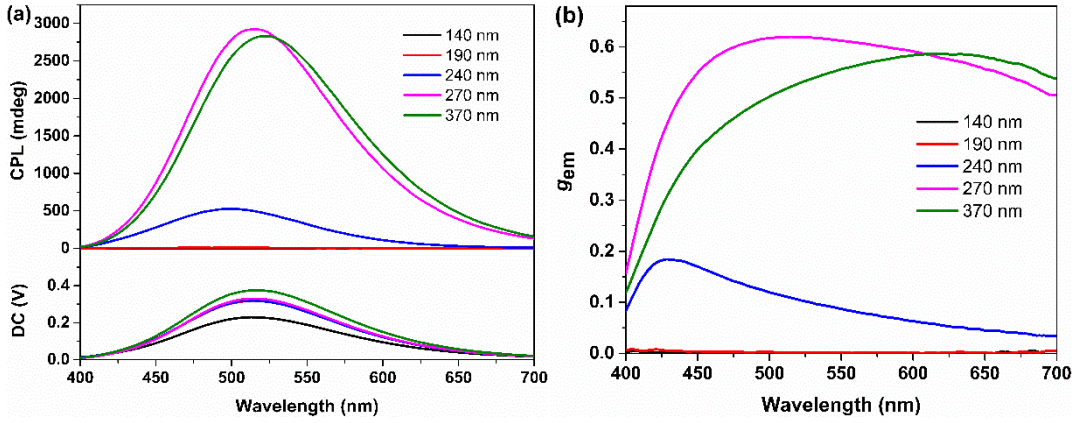

Figure S11. (a) CPL spectra and (b) the plot g_{em} values of ***R*-M-(PyBO)$_4$-T** spin-coated from THF solutions of different concentrations (10, 20, 30, 40, 50 mg/mL, respectively).

11. POM and Optical microscope images of *R/S*-M (from DCM and THF solution) and *R*-M-(PyBO)$_4$-D/T.

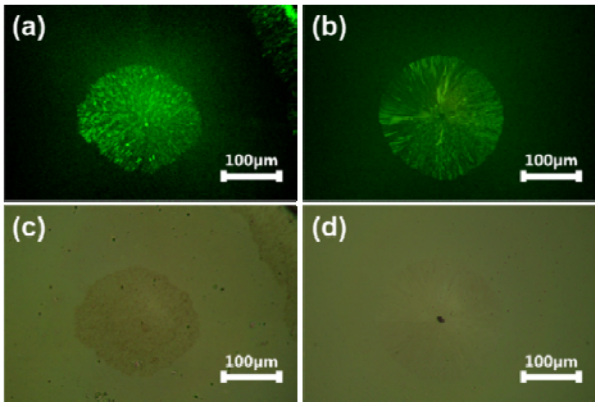

Figure S12. (a) POM images and (c) Optical microscope images of ***R*-M** film spin-coated from DCM solution (after 20 min); (b) POM images and (d) Optical microscope images of ***R*-M** film spin-coated from THF solution (after 20 min). All spin-coated films from 40 mg/mL solutions on quartz plates (1 cm × 3 cm) (1000 N/s, 30 s).

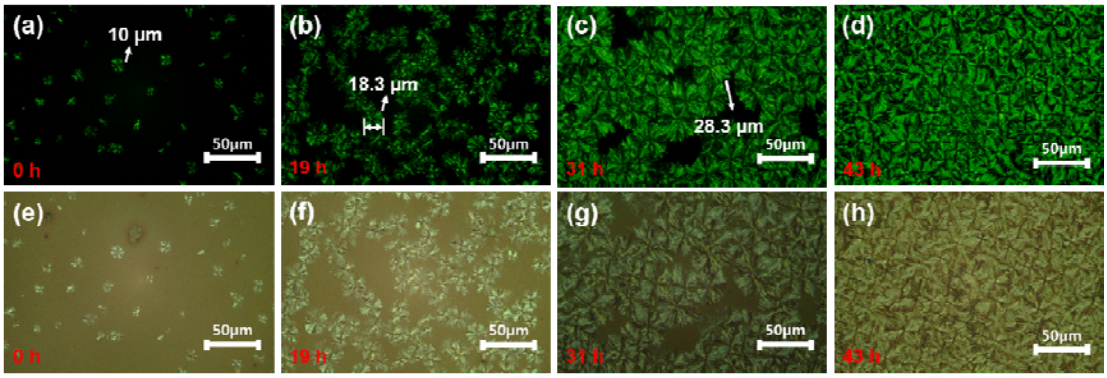

Figure S13. (a-d) POM images and (e-h) Optical microscope images of ***R*-M-(PyBO)$_4$-D** films spin-coated from DCM solutions (40 mg/mL) at different time.

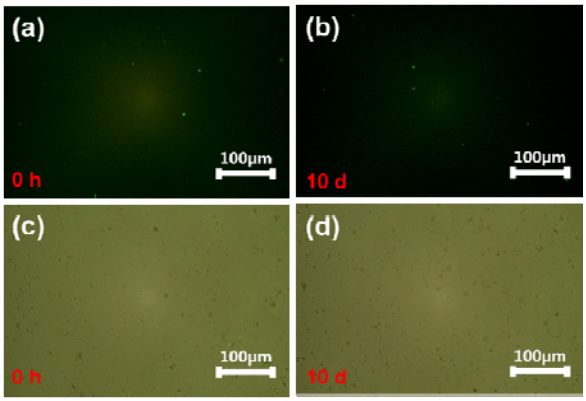

Figure S14. (a,b) POM images and (c,d) Optical microscope images of ***R*-M-(PyBO)$_4$-T** films spin-coated from THF solutions (40 mg/mL) at different time.

12. SEM images.

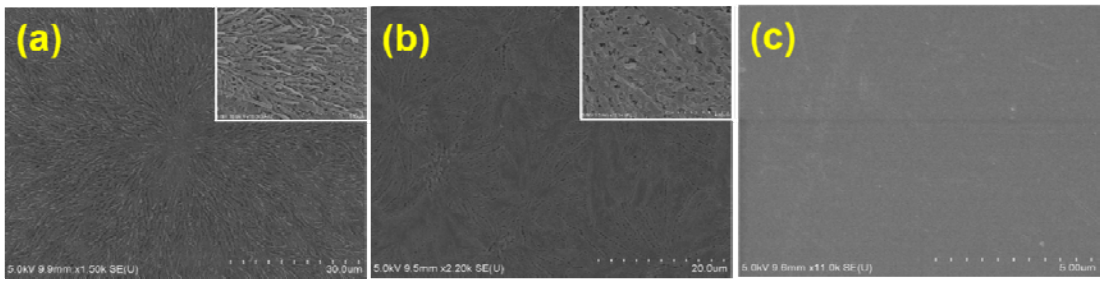

Figure S15. SEM images of (a) ***R*-M-(PyBO)$_4$**, (b) ***R*-M-(PyBO)$_4$-D** and (c) ***R*-M-(PyBO)$_4$-T** after 187 h, 45 h and 10 d, respectively. All spin-coated films from 40 mg/mL solutions on quartz plates (1 cm × 3 cm) (1000 N/s, 30 s).

13. XRD patterns.

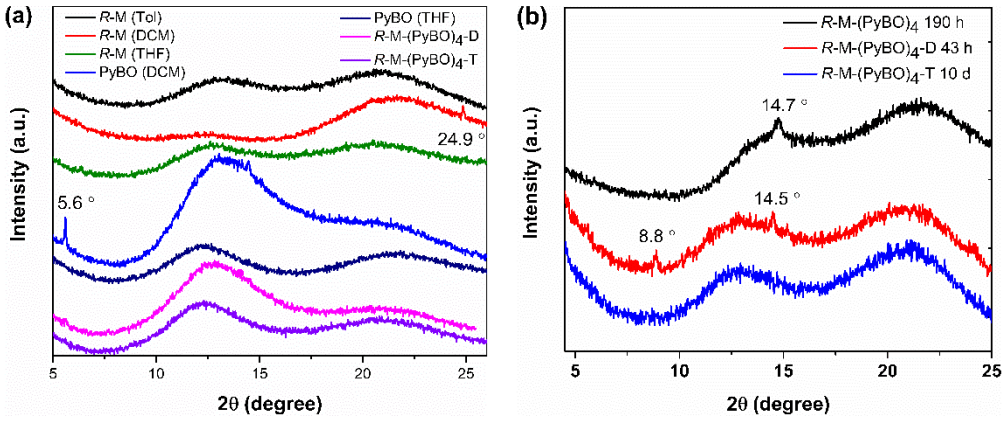

Figure S16. (a) XRD patterns of ***R*-M**, **PyBO** and ***R*-M-(PyBO)$_4$** fleshly films; (b) XRD patterns of ***R*-M-(PyBO)$_4$**, ***R*-M-(PyBO)$_4$-D** and ***R*-M-(PyBO)$_4$-T** in air for some time (h).

14. Comparison of the part of chiral excimer system.

Table S2. Comparison of the part of chiral excimer system

Compound	state	λ_{em} (nm)	$\lvert g_{em}\rvert$	reference
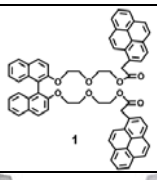	$CHCl_3$ solution	480	7.8×10^{-4}	*Chem. Commun.* **2014**, *50*, 13228
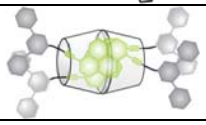	ammonia-containing H_2O at ca. pH 9.5.	528	1.5×10^{-2}	*Angew. Chem. Int. Ed.* **2014**, *53*, 14392

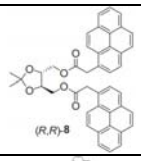	$CHCl_3$ solution	460	8.9×10^{-4}	*Chem. Commun.* **2015**, *51*, 8237
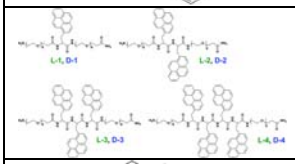	$CHCl_3$ solution	460	$0.3 \sim 1.0 \times 10^{-2}$	*Org. Biomol. Chem.* **2015**, *13*, 11426.
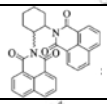	MeOH solution	470	3.7×10^{-2}	*Chem. Eur. J.* **2016**, *22*, 9519.
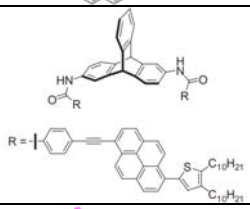	hexane/THF (95:5) solution	520	1.4×10^{-3}	*Org. Biomol. Chem.* **2017**, *15*, 8440.
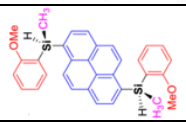	CH_2Cl_2 solution	500	8×10^{-3}	*J. Org. Chem.* **2017**, *82*, 6108.
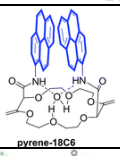	CH_3CN with $Ba(ClO_4)_2$.	490	9×10^{-3}	*Chem. Sci.* **2018**, *9*, 7043.
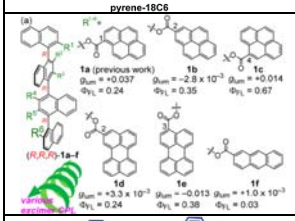	CH_2Cl_2 or THF solution	Blue to orange	$0.1 \sim 1.4 \times 10^{-2}$	*J. Am. Chem. Soc.* **2019**, *141*, 6185.
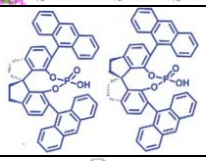	THF/H_2O (1/9) solution	460	2.9×10^{-2}	*Chem. Sci.* **2019**, *10*, 6821.
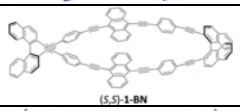	$CHCl_3$ solution	680	1.1×10^{-2}	*Chem. Eur. J.* **2019**, *25*, 9211.
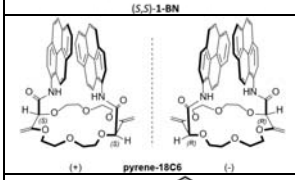	CH_3CN solution	490	9×10^{-3}	*Angew. Chem. Int. Ed.* **2019**, *58*, 6952.
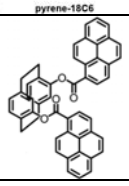	KBr-pellet	513	3.9×10^{-3}	*RSC Adv*. **2020**, *10*, 11335.

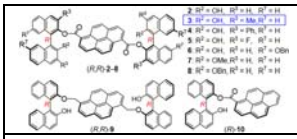	Toluene or DMSO solution	538	1.2×10^{-2}	*J. Am. Chem. Soc.* **2020**, *142*, 1774.
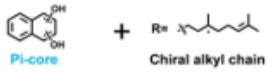	2 % Planar anthracene in Nap2 (molar ratios)	406	5.2×10^{-2}	*Angew. Chem. Int. Ed.* **2021**, *60*, 3745.
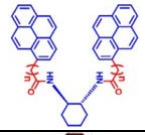	DMF solution	493~474 nm	$0.3\sim2.64 \times 10^{-2}$	*Angew. Chem. Int. Ed.* **2021**, *60*, 19451.
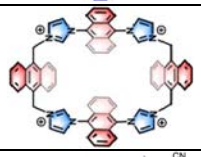	with ATP (0-1.5 equiv) in H_2O solution	550	1×10^{-2}	*Angew. Chem. Int. Ed.* **2021**, *60*, 15354.
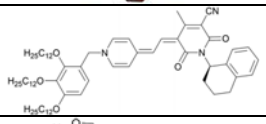	MCH solution	700	1.1×10^{-2}	*Chem. Sci.* **2021**, *12*, 12302.
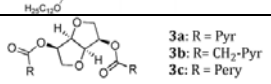	CH_2Cl_2 solution	500	9.6×10^{-3}	*Chem. Eur. J.* **2022**, e202104226. (10.1002/chem.202104226)
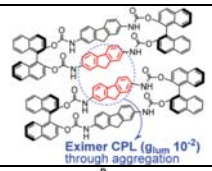	THF solution	370	1.1×10^{-2}	*Chem. Commun.* **2022**, *58*, 1029.
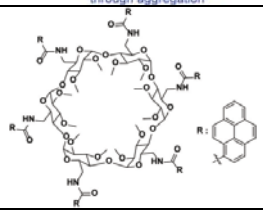	CH_2Cl_2 solution	486	1.2×10^{-2}	*Angew. Chem. Int. Ed.* **2022**, *61*, e202114700. (10.1002/ange.202114700)

170
171

15. ^{1}H and ^{13}C NMR Spectra of Compounds.

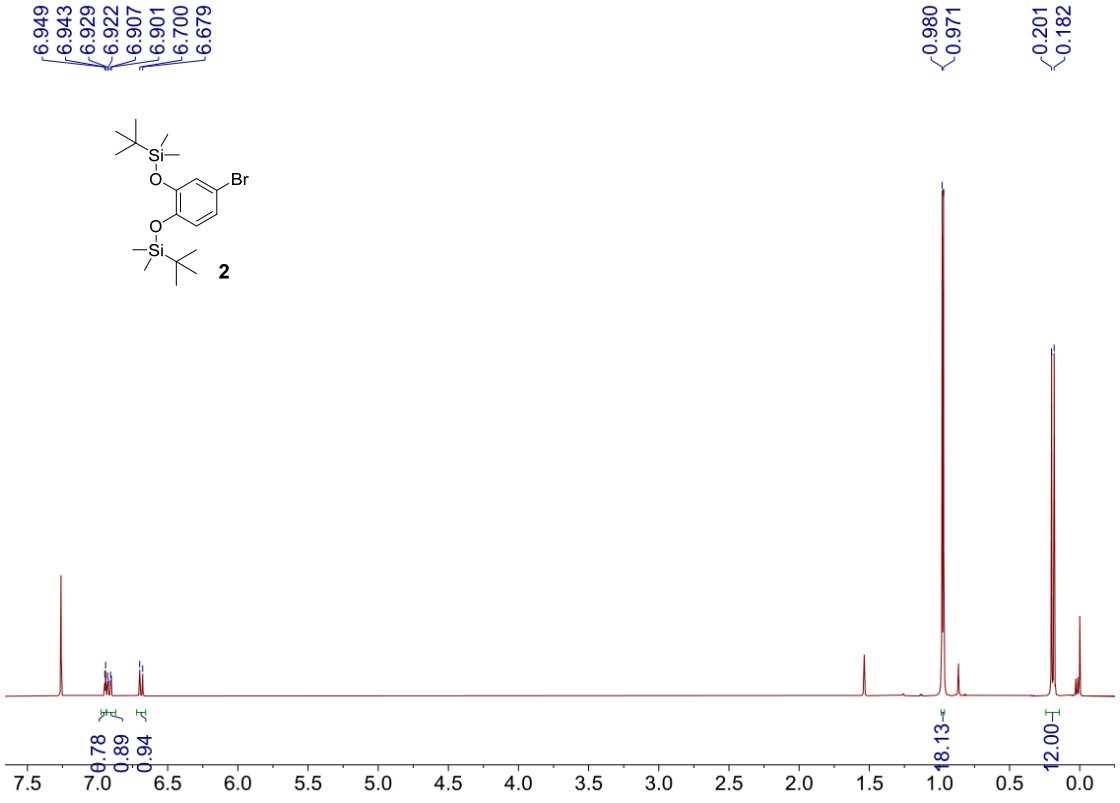

Figure S17. ^{1}H NMR spectrum of compound **2** (400 MHz, $CDCl_3$).

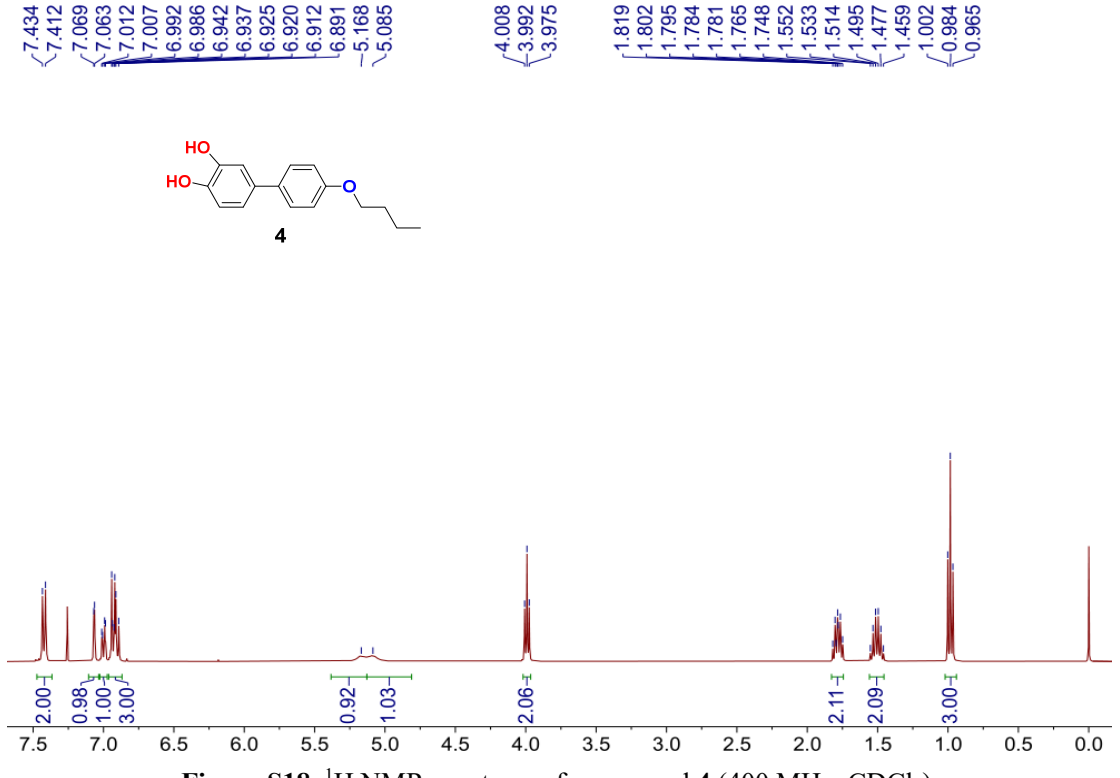

Figure S18. ^{1}H NMR spectrum of compound **4** (400 MHz, $CDCl_3$).

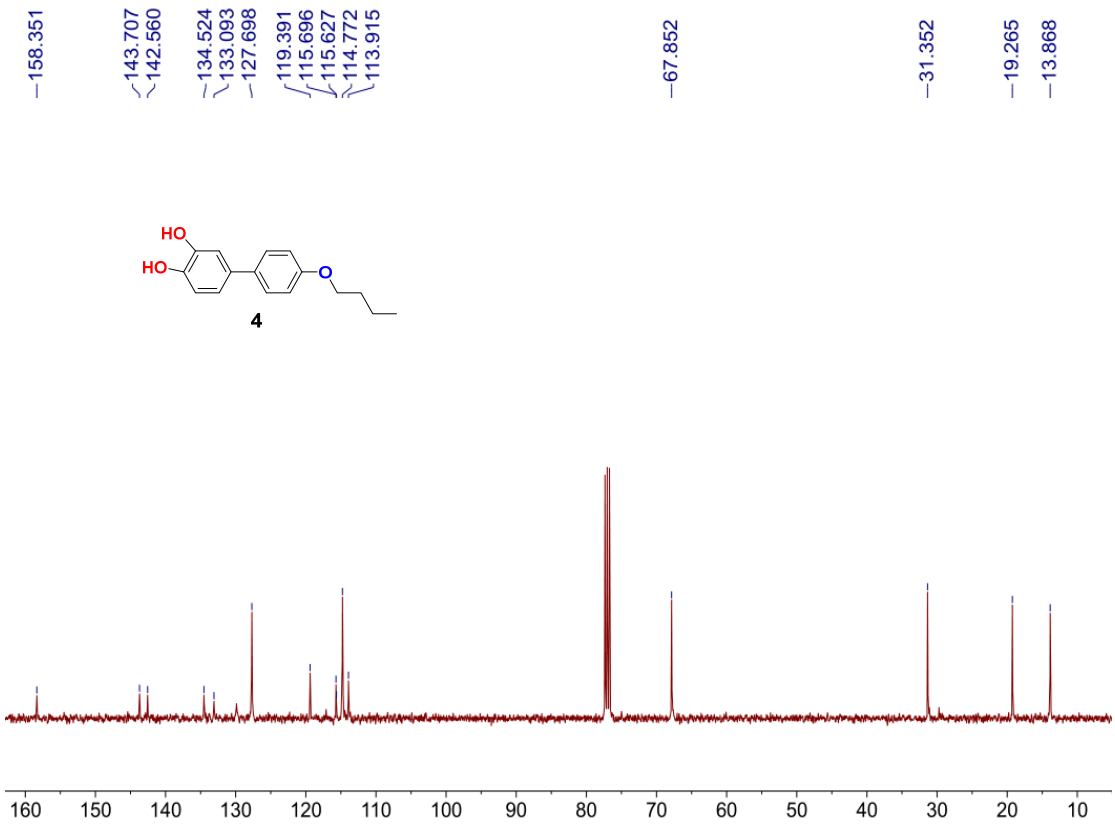

Figure S19. ^{13}C NMR spectrum of compound **4** (100 MHz, $CDCl_3$).

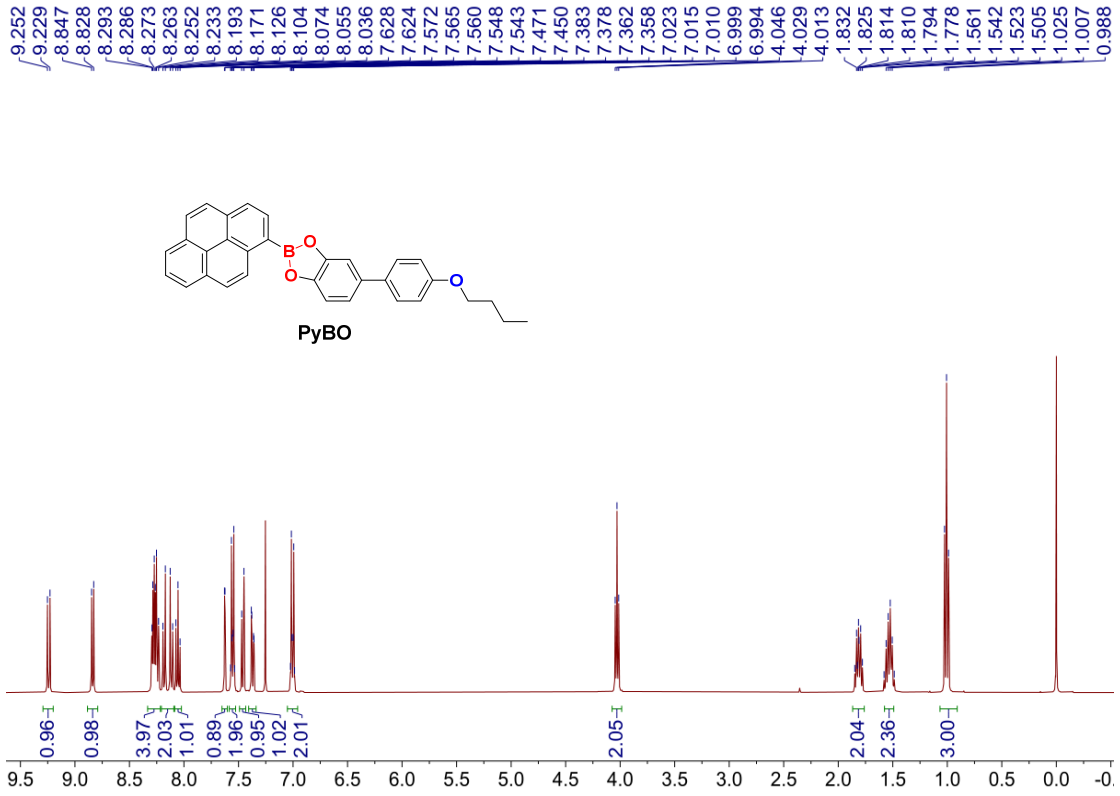

Figure S20. ^{1}H NMR spectrum of compound **PyBO** (400 MHz, $CDCl_3$).

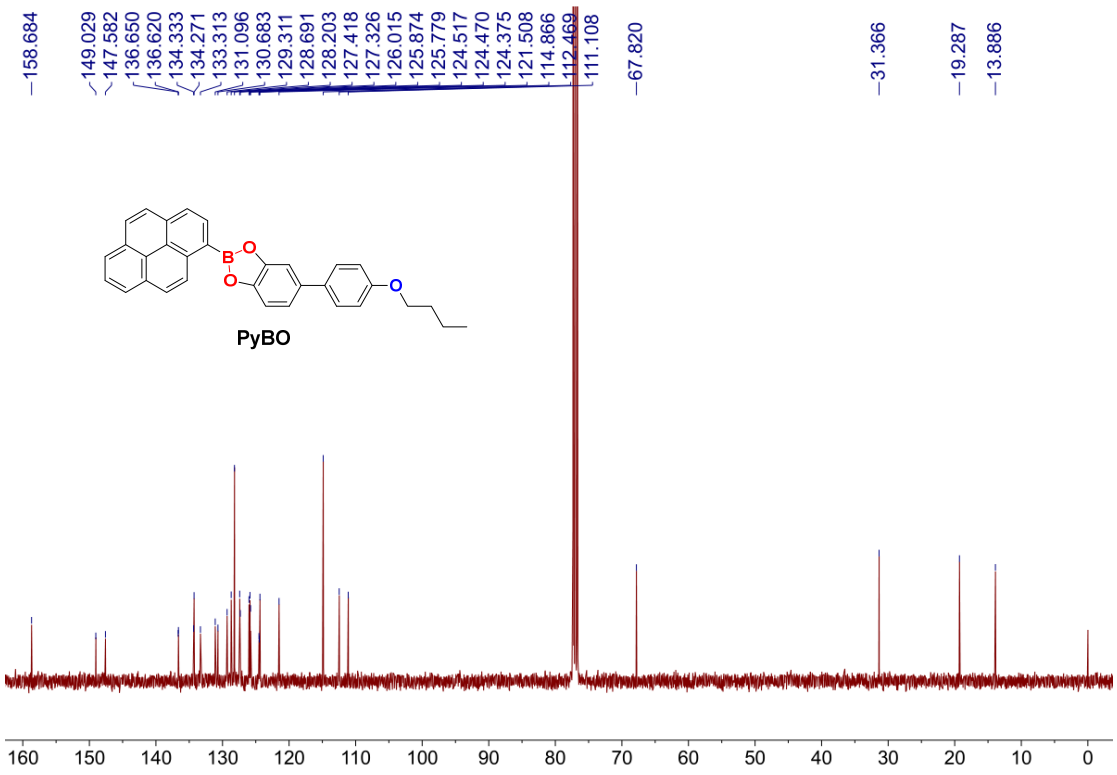

Figure S21. ^{13}C NMR spectrum of compound **PyBO** (100 MHz, $CDCl_3$).

16. Reference

(1) Li, Y., Urbas, A. & Li, Q. Reversible light-directed red, green, and blue reflection with thermal stability enabled by a self-organized helical superstructure. *J. Am. Chem. Soc.* **134,** 9573-9576 (2012).

(2) Zhang, Y. et al. Inverted circularly polarized luminescence behavior induced by helical nanofibers through chiral co-assembly from achiral liquid crystal polymers and chiral inducers. *ACS Nano* **16,** 3173-3181 (2022).

(3) Schrçder, P. et al. Neuritogenic militarinone-inspired 4-hydroxypyridones target the stress pathway kinase MAP4K4. *Angew. Chem. Int. Ed.* **54,** 12398-12403 (2015).